The Meteoritical Society

Meteoritics & Planetary Science 48, Nr 11, 2333–2349 (2013)
doi: 10.1111/maps.12135

The origin of eucrites, diogenites, and olivine diogenites: Magma ocean crystallization and shallow magma chamber processes on Vesta

Ben E. MANDLER[1*] and Linda T. ELKINS-TANTON[2]

[1]Department of Earth, Atmospheric and Planetary Sciences, Massachusetts Institute of Technology, 77 Massachusetts Avenue, Cambridge, Massachusetts 02139, USA
[2]Department of Terrestrial Magnetism, Carnegie Institution for Science, Washington, District of Columbia 20015, USA
*Corresponding author. E-mail: bmandler@mit.edu

(Received 02 April 2013; revision accepted 30 April 2013)

Abstract–The asteroid 4 Vesta is one of the very few heavenly bodies to have been linked to samples on Earth: the howardite-eucrite-diogenite (HED) meteorite suite. This large and diverse suite of meteorites provides a detailed picture of Vesta's igneous and postigneous history. We have used the range of igneous rock types and compositions in the HED suite to test a series of chemical models for solidification processes following peak melting (magma ocean) conditions on Vesta. Fractional crystallization cannot have been a dominant early process in the magma ocean because it leads to excessive Fe-enrichment in the melt. Models that are dominated by equilibrium crystallization cannot produce orthopyroxene cumulates (diogenites). Our best models invoke 60–70% equilibrium crystallization of a magma ocean followed by continuous extraction of the residual melt into shallow magma chambers. Fractional crystallization in these magma chambers combined with continuous or periodic addition of more melt from the slowly compacting crystal mush (magmatic recharge) can produce all of the igneous HED lithologies (noncumulate and cumulate eucrites, diogenites, dunites, harzburgites, and olivine diogenites). Magmatic recharge can also explain the narrow range in eucrite compositions and the variability of incompatible trace element concentrations in diogenites. We predict an internal structure for Vesta that permits excavation of the HEDs during the formation of the Rheasilvia basin, while remaining consistent with observations from the Dawn mission and most impact models.

INTRODUCTION

The asteroid 4 Vesta is widely considered to be the parent body of the howardite-eucrite-diogenite (HED) meteorite suite (McCord et al. 1970; Binzel and Xu 1993; McSween et al. 2011). The main igneous lithologies are noncumulate eucrites (pigeonite-plagioclase basalts) and diogenites (orthopyroxene cumulates), thought to represent Vesta's upper and lower crust, respectively (e.g., Ruzicka et al. 1997). Howardites are impact breccias, composed predominantly of eucrite and diogenite clasts. Rarer rock types include cumulate eucrites and olivine-bearing diogenites. This large and diverse suite of meteorites provides a detailed picture of Vesta's igneous and postigneous history. This paper presents a new attempt to develop a model for Vesta's early igneous history that can explain the range of rock types and compositions in the HED suite. With the wealth of information that is coming out of the Dawn mission, which orbited Vesta for a year beginning in July 2011, such models can be tested in an increasingly rigorous and detailed fashion.

Any model of Vesta's early evolution is subject to four major constraints: chronological, thermal, petrological/chemical, and physical. First, we will review the major chronological and thermal constraints on the early igneous history of Vesta, before discussing the range of existing hypotheses for HED formation. We then present modeling work in which we look at a number of scenarios for the solidification of a magma ocean on Vesta, and discuss these in the context of existing models, physical constraints, and Dawn data. Models that cannot explain the range of HED lithologies are defined, and a new model is proposed for

HED genesis. Finally, we show that all of the HEDs can be excavated during the formation of the Rheasilvia basin without violating observations from the Dawn mission or predictions from impact models.

CHRONOLOGY OF EARLY PROCESSES ON VESTA

Absolute and relative ages of eucrites both indicate that Vesta accreted and was heated very rapidly. Eucrites exhibit siderophile depletions that indicate the formation of an iron-rich core prior to their crystallization (Palme and Rammensee 1981; Righter and Drake 1997). The age of eucrites therefore provides a point in time by which Vesta must have accreted, melted, segregated a metallic core, and crystallized magma at its surface. U-Pb and ^{207}Pb-^{206}Pb ages of zircons in eucrites suggest that this had occurred by 4554 ± 7 Ma (approximately 7–20 Myr after the formation of CAIs at 4568 Ma [Misawa et al. 2005]). ^{53}Cr excesses in eucrites due to the decay of ^{53}Mn ($t_{1/2}$ = 3.7 Myr) yield an age for some eucrites of 2–4 Myr after CAIs (Lugmair and Shukolyukov 1998; Trinquier et al. 2008). Evidence for the presence of the short-lived radioisotopes ^{60}Fe ($t_{1/2}$ = 2.62 Myr) and ^{26}Al ($t_{1/2}$ = 0.7 Myr) in both eucrites and diogenites (Shukolyukov and Lugmair 1993; Quitté et al. 2011; Schiller et al. 2011) further shows that Vesta accreted, melted, and differentiated within the first few million years of the solar system.

Younger ages for HEDs are more difficult to interpret because isotopic closure is delayed by slow cooling at depth and isotopic clocks can be reset by impacts. For example, unbrecciated eucrites consistently yield Ar-Ar ages around 4.48 Ga (Bogard and Garrison 2003), but these only record the K-Ar closure temperature (approximately 200 °C for plagioclase). These younger apparent ages may therefore be due to slow crustal cooling or impact-induced reheating on Vesta (Bogard and Garrison 2003; Kleine et al. 2005).

The youngest eucrite ages are all obtained by Ar-Ar dating, which is easily reset by impacts. Brecciated eucrites, while yielding CAI-like Mn-Cr, Hf-W, and Pb-Pb ages, commonly exhibit a range of Ar-Ar ages between 3 and 4 Ga (Bogard and Garrison 2003). Young ages have also been obtained from Sm-Nd dating of eucrites, both cumulate and noncumulate, with ages spreading from 4.57 to 4.3 Ga (Blichert-Toft et al. 2002; Nyquist et al. 2004), for which similar resetting arguments have been invoked. The overriding message from the full suite of chronometers applied to eucrites is that magmatic activity had essentially ceased within 10–20 Myr after the formation of CAIs. This has important implications for the early thermal state of Vesta.

Vesta's Early Thermal History

To account for the age and extent of igneous activity on Vesta, heating must have been rapid and relatively short-lived. The last Vesta-building planetesimal collisions (projectiles potentially 10s of km across) may have been sufficiently energetic to cause significant local melting (Davison et al. 2012). The release of gravitational potential energy during core formation would also have provided some additional heat. However, impacts and core formation were probably minor heat sources compared with the decay of ^{26}Al ($t_{1/2}$ = 0.7 Myr), which would have been a major heat source on Vesta because of its rapid early accretion while ^{26}Al was still abundant.

A number of studies have attempted to model the early thermal evolution of asteroids based on the decay of ^{26}Al, including two specifically focused on Vesta (Ghosh and McSween 1998; Gupta and Sahijpal 2010). The first-order result of these models is that ^{26}Al was a potent heat source capable of inducing high degrees of melting early in Vesta's history. However, the fine details of Vesta's thermal history cannot yet be determined from thermal models because existing models do not adequately deal with convective heat transfer or the dynamics of an upper boundary layer that is prone to impact heating, foundering, and reincorporation into the interior. Instead, many workers have attempted to use the chemistry and petrology of HEDs to differentiate between potential thermal histories, specifically to differentiate between low and high degrees of melting.

Existing Petrogenetic Models for HEDs

Existing petrogenetic models for the igneous HED lithologies (eucrites and diogenites) can be split into two main groups: partial melting versus extensive melting (magma ocean).

The main argument for partial melting models stems from early experimental work on noncumulate eucrites, which found that their major-element compositions cluster around the 1-atmosphere plagioclase—olivine—low-Ca-pyroxene peritectic (Stolper 1975). This was used to suggest that eucrites may have formed by partial melting of a relatively homogeneous chondritic source, which would indeed produce melts of a relatively constant composition around the peritectic. However, we propose that noncumulate eucrites cannot be partial melts, but must instead be residual melts left over after the formation of diogenites by fractional crystallization. The argument for this is both physical and chemical. Diogenites are orthopyroxene cumulates, so their crystallization must leave a residual liquid. This residual liquid is less dense than the diogenites that crystallize

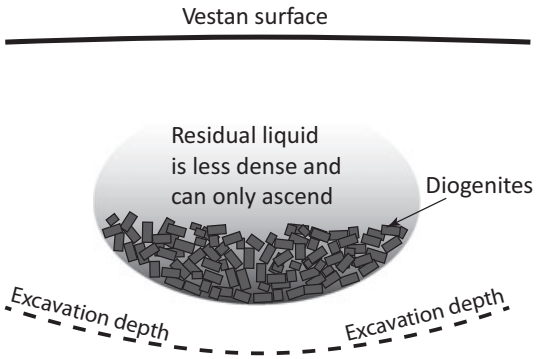

Fig. 1. Schematic showing how the residual liquid from diogenite formation must crystallize at shallower levels in Vesta and therefore must have been excavated along with the diogenites and transported to Earth. These residual liquids must be eucrites—see text for further details.

from it, so it must ultimately crystallize at shallower depths than diogenites (Fig. 1). Therefore, any impact that excavated the diogenites must also have excavated these residual liquids. Any liquid derived from a chondritic mantle can only crystallize at most approximately 50% of its mass as orthopyroxene, so the residual liquids must be at least as abundant as diogenites. Furthermore, because these liquids crystallized closer to the vestan surface, they should be more abundant than diogenites in the meteorite collection and at least as abundant as diogenitic material on the surface of Vesta. Eucrites meet both of these criteria (e.g., De Sanctis et al. 2012). We will also show later in this paper that the liquids that crystallize diogenites become eucritic in composition after the diogenites have crystallized out of them.

These physical and chemical arguments, combined with the fact that there are no other candidates for these residual liquids in the global meteorite collection, make it clear that eucrites cannot be partial melts and must be residual liquids. It follows that any model trying to explain diogenites or eucrites must explain both at the same time because they must be genetically linked. Stolper (1977) tried to circumvent this problem by suggesting that diogenites could form from partial melts of a depleted vestan mantle that had previously partly melted to form eucrites. These new melts would be close to pure orthopyroxene in composition and so could crystallize as plutons in the vestan crust without leaving a eucritic residual liquid. This received some support from Mittlefehldt (1994) and Fowler et al. (1995), who showed that diogenites exhibit a large and systematic variation in incompatible trace element (ITE) concentrations. ITE variations are decoupled from major-element concentrations and cannot be explained by fractional crystallization of a single liquid. Shearer et al. (1997) suggested that this could be explained by fractional melting of the depleted vestan mantle. However, with Vesta heating up over time due to ^{26}Al decay, the most ITE-enriched diogenites would form first, as the first low-degree melts would remove the ITEs from the mantle. Later melts would then have progressively ITE-depleted compositions as they formed from a progressively depleted mantle. Recent work by Schiller et al. (2011) has shown that the opposite is observed—younger diogenites are more ITE-enriched. We will show later that this supports a fractional crystallization origin for the diogenites, with the eucrites as their residual melts.

With thermal models showing how powerful a heat source ^{26}Al decay can be (e.g., Hevey and Sanders 2006), a magma ocean origin for eucrites and diogenites has grown in popularity, although this idea is not a particularly recent one (Ikeda and Takeda 1985; Righter and Drake 1997; Ruzicka et al. 1997; Warren 1997). Magma ocean models have several important advantages over partial melting models. First, homogenization of the vestan interior by vigorous mixing in a magma ocean can explain the homogeneity in Ti and O isotopes among the HEDs (e.g., Zhang et al. 2012; Greenwood et al. 2013). This homogeneity is difficult to achieve in a partly molten body that retains its solid framework, as observed in the partly molten but unequilibrated ureilite parent body (Clayton and Mayeda 1988; Singletary and Grove 2003). Second, inverse modeling of siderophile elements in eucrites suggests that, if Vesta has a chondritic bulk composition in terms of siderophile elements, it should have been approximately 70% molten at the time of core segregation (Righter and Drake 1997), which must have preceded eucrite formation. Third, a magma ocean could wipe out any lithological signature of Vesta's chondritic building blocks. This is particularly important because Dawn has not observed a large amount of relict undifferentiated material on Vesta (e.g., De Sanctis et al. 2012), which should exist if Vesta only experienced partial melting.

We will discuss magma ocean models for HED petrogenesis in more detail in the discussion section of this paper, where we compare our results with existing models. However, a key issue to note here is that magma ocean models require an alternative mechanism to explain the narrow range in noncumulate eucrite compositions. Ikeda and Takeda (1985) favored a model in which a critical amount of cooling prevented a eucritic crust from foundering back into the magma ocean. This crust would represent most eucrites. Ruzicka et al. (1997) suggested that a fractional crystallization stage, producing dunite and diogenite, would be followed by an equilibrium crystallization stage producing eucrites as basalts or gabbros of an

approximately constant composition. Conversely, Righter and Drake (1997) suggested that equilibrium crystallization of a magma ocean would be followed by extraction and mass-eruption of the eucritic residual melt after 80% crystallization. Warren (1997) proposed that a moderate amount of fractional crystallization of eucritic melt would not significantly change its composition because the crystal assemblage would be similar in composition to the liquid. We will argue here for an alternative mechanism that can better explain the compositions of HED lithologies: magmatic recharge of shallow magma chambers from an underlying compacting crystal mush after extensive magma ocean crystallization.

Model Setup

Estimates of the bulk composition of Vesta's mantle came from a variety of sources (Table 1). For all compositions with $Na_2O > 0.1$ wt% and $K_2O > 0.01$ wt%, Na_2O and K_2O were reduced to these values to reflect the extreme volatile depletion observed in HED meteorites, which is an unresolved problem that we do not investigate here. Only major and minor elements were modeled because only they dictate crystallization/melting behavior, and because their initial abundances—and their abundances in HEDs—are better constrained than trace elements. The starting assumption for each model was that the mantle was entirely molten, but similar results were achieved as long as the initial melt fraction was >60%. For each bulk composition, the chemical evolution of the melt was tracked for a variety of crystallization scenarios using the MELTS program (Ghiorso and Sack 1995; Asimow and Ghiorso 1998). MELTS is well calibrated for the simple crystallization paths of ultramafic and mafic melts at $f_{melt} > 0.1$ and low pressures, so it should closely approximate the true crystallization sequence up to at least 90% crystallization.

Both one-step and two-step models were tested. One-step models tracked the evolving liquid and solid compositions during either fractional or equilibrium crystallization (hereafter FC and EC, respectively) at a pressure of 500 bars (approximately 60 km depth in Vesta—corresponding approximately to the average depth in the magma ocean) until only 10 wt% melt remained. Equilibrium crystallization is the same as equilibrium melting in reverse, so the EC models are functionally also equilibrium melting models. Two-step models comprised partial crystallization at 500 bars, followed by extraction and subsequent crystallization of the residual melt at 200 bars (approximately 25 km depth in Vesta—corresponding to what is now the midlower crust). Models that remelted cumulates from the FC model were also considered, but these consistently failed to produce melts that can be related to eucrites or diogenites (Fig. 2).

Table 1. Bulk silicate Vesta compositions used in models.

	RD	DW	RZ	LOD	BD
SiO_2	46.01	46.44	45.54	46.08	45.83
TiO_2	0.15	0.16	0.18	0.14	0.16
Al_2O_3	3.11	3.29	3.30	2.93	2.86
Cr_2O_3	0.67	0.87	0.85	0.69	0.67
FeO	18.18	14.88	14.40	17.47	18.30
MgO	29.25	31.66	32.81	30.16	29.68
CaO	2.49	2.58	2.79	2.39	2.37
Na_2O	0.11	0.10	0.10	0.10	0.10
K_2O	0.01	0.01	0.01	0.01	0.01
Mg#	74.2	79.1	80.2	75.5	74.3

RD = Righter and Drake (1997) 0.30CV-0.70L model with volatile depletion; DW = Dreibus and Wänke (1980); RZ = Ruzicka et al. (1997) HED-CI model; LOD = Lodders (2000) OIM model; BD = Boesenberg and Delaney (1997) 30 Murch-70 H model; Mg# = molar MgO/(MgO + FeO).

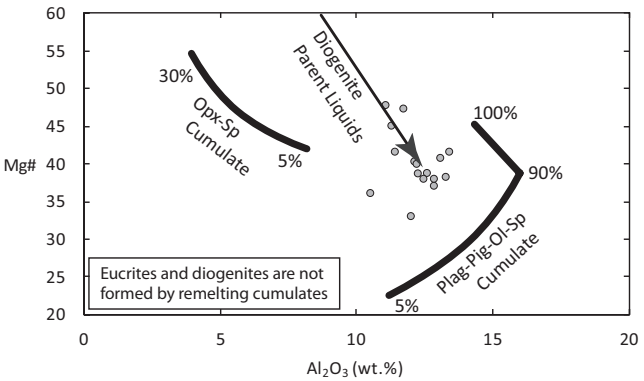

Fig. 2. Mg# (molar MgO/(MgO + FeO)) versus Al_2O_3 content of melts produced by remelting cumulate layers after fractional crystallization of a DW-composition magma ocean. Opx-Sp cumulate = melts of a cumulate composition produced after 66 wt% crystallization of the magma ocean. Plag-Pig-Ol-Sp cumulate = melts of a cumulate composition produced after 80 wt% crystallization. Percent values next to curves indicate extent of remelting. Circles are compositions of noncumulate eucrites (except Ibitira) from Kitts and Lodders (1998). "Diogenite Parent Liquids" line represents liquid compositions that could feasibly produce both diogenites and eucrites.

RESULTS

One-Step Models

Figure 3 shows the proximity in composition space of modeled liquids to eucritic compositions. The target eucrite composition is Sioux County, chosen as the

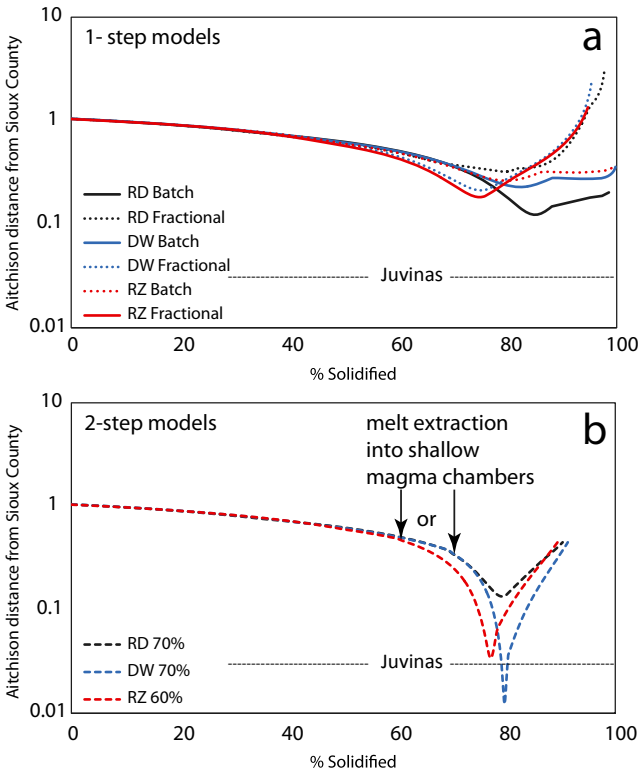

Fig. 3. Proximity in composition space of modeled evolving magma ocean liquids to the composition of Sioux County (Palme et al. 1978) in terms of Aitchison distance. (a) 1-step models; (b) 2-step models. For perspective, the Aitchison distance of Juvinas (Wänke et al. 1972) from Sioux County is also shown. Juvinas and Sioux County are very similar in composition, and both represent "primitive" eucrites. Models are deemed to have successfully reproduced eucrite compositions if they closely approach or cross the Juvinas line. In two-step models (b), melt is extracted into shallow magma chambers after either 60 or 70% solidification.

target because it is one of the most primitive (high Mg# (molar MgO/MgO + FeO), low Ti) noncumulate eucrites and its composition is well constrained. The choice of target composition does not significantly affect the results because there is little variation in the major-element composition of eucrites—different target choices only shift the best-fit minima to approximately 1% less or more solidification. For two-step models, the degree of crystallization corresponding to the start of the second step was varied in 10% increments from 50 to 80%. Melt extraction prior to 50% made all models look like one-step FC models, while extraction after 80% did not produce diogenites. Only models for RD, DW, and RZ compositions (Table 1) are shown because LOD and BD compositions are sufficiently similar to RD that they yield very similar results. In Fig. 3b, the most successful two-step model is shown for each of the three bulk compositions. The proximity in composition space of the evolving liquid to the eucrite target was measured by the Aitchison distance, defined in this case as:

$$\sqrt{\sum_{i=1}^{5}[\mathrm{clr}(x)_i - \mathrm{clr}(y)_i]^2} \text{ where } \mathrm{clr}(x) = \begin{pmatrix} \log\left(\frac{x_1}{g(x)}\right) \\ \vdots \\ \log\left(\frac{x_5}{g(x)}\right) \end{pmatrix}$$

where $g(x)$ is the geometric mean of the elements in x; x and y are the model and target compositions; and elements 1 through 5 are weight percent values of SiO_2, Al_2O_3, MgO, FeO, and CaO. These components make up 98–99 wt% of the liquids in question. Minor components Na_2O, K_2O, TiO_2, and Cr_2O_3 were not used because Aitchison distances are highly sensitive to large relative changes in small values, and therefore sensitive to the poor constraints we have on minor element abundances in Vesta.

The Aitchison distance provides a measure of how far two points are from one another in composition space. In this sense, it is much like the normalized root-mean-square deviation (NRMSD). The difference is that the NRMSD only produces a true mathematical difference or "distance" in unconstrained Euclidian space and so is not strictly appropriate for measuring distances in composition space, which is constrained by the fact that all values must sum to 1. Compositions are therefore defined as the ratio of elements to one another. The Aitchison distance measures differences in ratios and so is a more appropriate measure of distance in composition space than the NRMSD (Aitchison 1986).

Figure 3 and Table 2 show that EC models generally produce eucrite-like compositions in terms of all elements except Mg and Fe, which are highly dependent on the choice of bulk Vesta composition, core size, and degree of crystallization. Some iteration of almost any one-step EC model can produce a true eucritic liquid. This is not surprising; any chondritic liquid that has lost an Fe-rich core and experienced 70–90% crystallization will be basaltic. All that is required for this basaltic composition to also be eucritic is volatile depletion (to explain low Na and K) and the "correct" Mg# of the starting liquid, which is a function of both bulk composition and core size/composition. However, one-step EC models cannot produce both eucrites and diogenites because diogenites are cumulates, which are products of FC.

Figure 3 and Table 2 show that FC models never closely approach the target compositions because the melts are too Fe-rich. While FC models do produce orthopyroxene cumulates, the removal of these cumulates from the melt drives the melt composition to

Table 2. Composition of Sioux County and closest approaches to this composition for each of the models in Fig. 3.

		1-Step Batch			1-Step Fractional			2-Step Batch then Fractional		
	Sioux County[a]	RD	DW	RZ	RD	DW	RZ	RD 70%[b]	DW 70%	RZ 60%
SiO_2	49.2	49.6	50.9	51.3	42.5	44.1	44.5	45.9	48.8	49.0
TiO_2	0.58	0.86	0.80	0.81	0.43	0.61	0.68	0.67	0.73	0.75
Al_2O_3	13.1	13.7	13.3	12.8	8.1	11.1	11.2	11.9	13.2	12.5
Cr_2O_3	0.32	0.22	0.26	0.27	0.71	0.33	0.31	0.27	0.23	0.25
FeO	18.4	15.6	13.1	12.4	31.9	28.0	26.5	24.3	18.9	19.5
MgO	6.9	8.7	10.3	10.9	9.3	6.4	6.6	6.6	7.0	6.8
CaO	10.4	10.6	10.7	10.9	6.7	9.1	9.7	9.7	10.6	10.7
Na_2O	0.41	0.72	0.55	0.49	0.32	0.40	0.39	0.52	0.49	0.43
K_2O	0.03	0.07	0.06	0.05	0.03	0.04	0.04	0.05	0.01	0.04
Mg#	40.0	49.9	58.4	61.1	34.2	28.9	30.6	32.8	39.6	38.4

[a]Composition of Sioux County is from Palme et al. (1978).
[b]Percent values for two-step models indicate the amount of solidification the magma has undergone prior to melt-mush segregation.

very high Fe, rapidly decreasing the Mg# of the melt. These melts are too Al+Ca-poor and too Fe-rich to form eucrites (Table 2). Equally, remelting of cumulates cannot produce appropriate eucrites or diogenites because the cumulates, and thus their melts, are either too Fe-rich or too Al+Ca-poor (Fig. 2).

Two-Step Models

In the two-step models, an initial EC stage at 500 bars (approximately 60 km depth) is followed by extraction of the residual melt and FC of this melt at 200 bars (approximately 25 km depth) in isolation from the solids produced in the first stage. FC-then-EC models were also tested but, while models in which FC is followed by EC are physically intuitive (we can imagine solidification rates at some point exceeding crystal settling rates), they consistently fail to produce eucrites and diogenites. They suffer the same problem as the one-step FC models (excessive Fe-enrichment at low Al+Ca) unless the FC stage is arrested prior to 40% crystallization, in which case the FC stage only crystallizes olivine and cannot produce orthopyroxene cumulates (diogenites).

Models in which an EC stage is followed by an FC stage are variably successful at producing eucrites and diogenites. Extracting the melt from the first stage too early (<60% crystallization) leads to excessive Fe-enrichment due to FC. Extracting the melt from the first stage too late (after 80% crystallization) results in a second-stage melt that is already eucritic and cannot form diogenites. However, extracting the melt from the first stage after 60–70% crystallization (1630–1680 K, depending on bulk composition) yields a second-stage melt that can produce diogenites by FC and end up at eucritic compositions (Fig. 3; Table 2). This model produces HEDs as long as the average pressure during the initial phase of magma ocean crystallization is high enough to allow cotectic crystallization of olivine and orthopyroxene. This is the case for pressures at least as low as 500 bars (Grove and Bartels 1992). The small pressure drop during subsequent melt extraction expands the olivine stability field and so triggers the crystallization of a small amount of olivine. This is important for the generation of olivine-bearing diogenites.

DISCUSSION

Improving on Previous Models

Two previous chemical models of magma ocean crystallization on Vesta have strongly guided this work. Ruzicka et al. (1997) proposed that FC of a magma ocean with the bulk composition of Dreibus and Wänke (1980) could produce both diogenites and eucrites. However, as noted by Righter and Drake (1997) and shown again in this study, the liquids produced by FC are too Fe-rich. While diogenite- and eucrite-like phase assemblages are produced during FC, the chemistry of these phases is not compatible with such an origin for diogenites and eucrites.

Righter and Drake (1997) instead proposed a model of extensive equilibrium crystallization followed by melt extraction and FC of the extracted melt. This is the same concept as that of the new model proposed later in this section. However, in the Righter and Drake model, EC prevails until 80% crystallization, after which point the residual melt is extracted and allowed to undergo FC. The lithologies produced are a harzburgite mantle, cumulate eucrites (from FC of the extracted melt), and noncumulate eucrites (from eruption of the extracted melt). The orthopyroxenes produced in their model are diogenite-like in composition, but they are all in harzburgites with

>50 wt% olivine, whereas almost all diogenites have <10% olivine (Beck and McSween 2010). Righter and Drake (1997) claimed that true diogenites (>90% orthopyroxene) could be produced during the late stages of EC in the magma ocean (after approximately 70–80% crystallization), as olivine was resorbed and orthopyroxene crystallized. However, if this was truly an EC process then the bulk composition would be far too olivine-normative to exhaust the olivine and produce near-monomineralic diogenites. The only way to produce these diogenites in such a model is to extract the melt at this stage so that the olivine crystals are no longer controlling the bulk composition. This would make the magma much more orthopyroxene-normative and permit the formation of true diogenites. This is the essence of our proposed model, which requires earlier melt extraction, after 60–70% crystallization.

A complete model of melting and crystallization on Vesta must account not only for eucrites (cumulate and noncumulate) and diogenites, but also for the other lithologies in the HED suite. These include dunites (>90% olivine cumulates; Beck et al. 2011) and olivine-bearing diogenites (Sack et al. 1991; Beck and McSween 2010). The Righter and Drake model does not produce diogenites and only produces dunites near the core-mantle boundary, which has not been sampled by impact excavation. However, a modified version of the Righter and Drake concept can produce all of the lithologies in the HED suite.

Figure 4a shows the chemical evolution of the melt for the most successful EC-then-FC model in this study. Much like the Righter and Drake model, the magma ocean initially undergoes equilibrium crystallization of olivine (step 1–2) followed by olivine + orthopyroxene (step 2–3). However, in our model, the residual melt is extracted from the magma ocean after 60–70 wt% crystallization instead of 80% (for appropriate densities, 70% crystallization by mass is equivalent to 67% crystallization by volume). At this point, the melt is still on the olivine-orthopyroxene boundary and leaves behind a harzburgite mush as it ascends (step 3). After continued melt extraction, the mush that it leaves behind will ultimately form a harzburgite mantle with approximately 62% olivine, 34% orthopyroxene, and 4% spinel; this represents a minimum olivine content for our successful models, which can produce a mantle with up to 80% olivine. At the top of the crystal mush, the magma undergoes fractional crystallization. The small pressure drop during melt ascent expands the olivine primary phase volume such that a small amount of olivine + spinel crystallization occurs, forming a thin dunite layer. This dunite consists of approximately 98% olivine and approximately 2% spinel (chromite), broadly consistent with the only vestan dunite found thus far (Beck et al. 2011). This will be followed by orthopyroxene + spinel crystallization, forming diogenites (step 3–4), and pigeonite + plagioclase + spinel crystallization (step 4–5), forming cumulate eucrites. As diogenites and cumulate eucrites are forming by FC of the evolving liquid (steps 3–5), noncumulate eucrites are formed by large-scale eruption of the melt onto Vesta's surface.

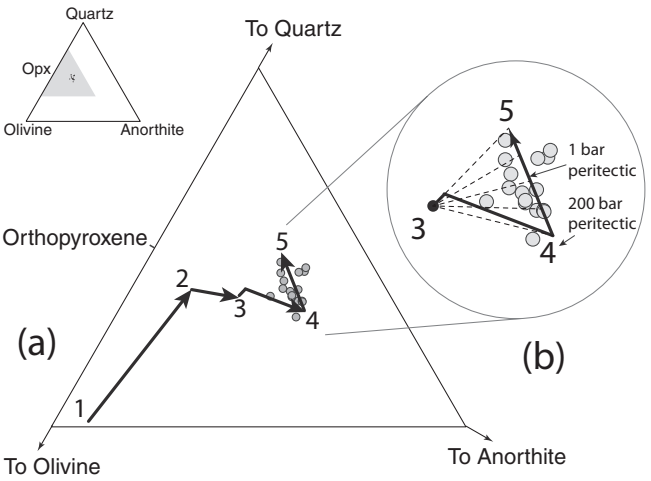

Fig. 4. a) Evolution of the melt for the best-fit model in this study, projected into the olivine-quartz-anorthite pseudoternary of Stolper (1975). Equilibrium crystallization phase: From (1) to (2), crystallization at 500 bars average pressure first produces olivine, then (2 to 3) olivine + orthopyroxene. Fractional crystallization phase: at (3), we have reached 70% total crystallization of the magma ocean. The melt is extracted from the crystal mush and undergoes fractional crystallization at 200 bars. From (3) to (4), a small amount of olivine crystallization is followed by orthopyroxene crystallization (formation of dunites, olivine diogenites, and diogenites). The stable pyroxene becomes pigeonite shortly before the melt reaches the plagioclase + pigeonite stability curve (4) very close to the plagioclase-pigeonite-olivine peritectic. From (4) to (5), most of the noncumulate eucrite melt compositions are created due to plagioclase + pigeonite fractional crystallization (formation of cumulate eucrites). Melts that are erupted form the noncumulate eucrites. Circles are all noncumulate eucrite compositions (except Ibitira) from Kitts and Lodders (1998). b) Inset showing how the recharge of magma chambers with liquid from the underlying crystal mush can maintain a limited range of compositions. Solid black circle represents the composition of liquid being extracted from the mush, which can mix with magma chamber liquids (which evolve along the black lines) to buffer compositions near the 1 bar peritectic. Dashed lines indicate the range of compositions produced by this process. Arrows point to the approximate locations of the 1 bar and 200 bar peritectics.

Generating the Narrow Range in Noncumulate Eucrite Compositions

The narrow range in noncumulate eucrite compositions can be explained by considering how

magma transport affects magma evolution. The best-fit models presented in Fig. 3 treat the melt as a single fractionating reservoir. In reality, evolving melt at the top of the crystal mush (base of the crust) will be continually "recharged" by more primitive melt ascending from the underlying mush. This is schematically illustrated in Figs. 4b and 8.

Consider a magma chamber that is evolving from steps 3–5 (Fig. 4b), changing its liquid composition as it produces cumulate assemblages (dunites, olivine diogenites, diogenites, and cumulate eucrites) by fractional crystallization. The composition of the evolving melt in the magma chamber follows the gray line in Fig. 4b. However, new melt continually or periodically ascends from the underlying crystal mush (see Fig. 8), adding more melt of composition 3 (Fig. 4b) to the magma chamber. This will bring the liquid composition back into the range where it will crystallize olivine (dunites), olivine + pyroxene (olivine diogenites), or, most commonly, only pyroxene (diogenites), before returning to plagioclase + pigeonite crystallization (cumulate eucrites).

As long as this process of magmatic recharge is operating, the melt composition will be buffered at a relatively constant composition, remaining within the region bounded by the dashed lines in Fig. 4b. This small range of compositions clusters around (but includes more silica-poor compositions than) the one-atmosphere olivine-pyroxene-plagioclase peritectic because the shallow vestan magma chambers are largely located at lower crustal levels (20–40 km = 160–330 bars). At this slightly elevated pressure, the peritectic moves slightly away from the silica apex in the olivine-quartz-anorthite pseudoternary (Fig. 4b). Magma chambers that were not as well buffered by recharge may have formed compositions such as the Nuevo Laredo eucrite trend, which progresses further down the pigeonite + plagioclase cocrystallization path (Stolper 1977). In addition, the variety of highly evolved compositions observed in howardites (Patzer 2013) may represent the dregs of these magma chambers, which would have fractionally crystallized all the way to high-Si, high-alkali, and high-(Fe/Mg) compositions.

Generating Compositional Variability in Diogenites

The process of magma recharge detailed above may also explain the wide yet systematic range in incompatible trace element (ITE) concentrations in diogenites (Fowler et al. 1995; Barrat et al. 2008), which are commonly decoupled from major-element concentrations (Mittlefehldt 1994; Barrat et al. 2008). Magmatic recharge of individual magma chambers progressively increases ITE concentrations while maintaining a relatively constant major-element composition. This is widely hypothesized on Earth (e.g., O'Hara 1977; DePaolo 1981) and could have been a fundamentally important process on Vesta.

One of the most common arguments against a purely FC origin for the large ITE variability in diogenites is that a single magma would have to crystallize 95% of its mass as orthopyroxene to produce the observed range of compositions (Mittlefehldt 1994; Shearer et al. 1997, 2010). With magma recharge constantly providing more ITEs and FC constantly enriching the magma chamber in ITEs, a large compositional range is easily achieved within each individual magma chamber. If magma recharge explains this variability, we would also expect incompatible element concentrations to increase over time. Figure 5 shows a good correlation between incompatible element concentration and age based on ^{26}Mg excesses in diogenites (Schiller et al. 2011).

Our model also reproduces the mineral compositions of cumulate HED lithologies (Fig. 6). Note that olivine and pyroxene compositions in modeled dunites and diogenites include more magnesian compositions than those observed in real diogenites and olivine diogenites. This is probably because our model assumes pure FC in the second stage. In reality, the interstitial liquid in large cumulate piles remains near equilibrium with the liquid in the overlying magma body until the trapped liquid fraction is very small (Tait et al. 1984; Tait and Jaupart 1996). As a result, cumulus minerals in lower crustal cumulates (dunites, olivine diogenites, and diogenites) would continue to grow and re-equilibrate (i.e., become more Fe-rich) until the porosity was too low for the cumulate pile and overlying magma to interact. In addition, the progression of some magma chambers to more evolved (higher Fe/Mg) compositions can explain the more Fe-rich cumulate eucrites.

There has been some recent debate over the potential role of assimilation in generating Eu anomalies in diogenites (Barrat et al. 2010; Mittlefehldt et al. 2012). If individual magma chambers were being constantly recharged, assimilation of surrounding rocks may be expected due to the release of latent heat during crystallization. We have not quantified this effect, but we expect it to be small because most of the surrounding rocks would also be cumulates from adjacent magma chambers. These cumulates would have solidi near to or even above the temperature of the magma chamber, so there would be very little assimilation. Later magma chambers could have assimilated some eucritic material that had been buried to magma chamber depths by overlying lava flows, although even eucrite assimilation would be minor. An alternative explanation for Eu anomalies in diogenites

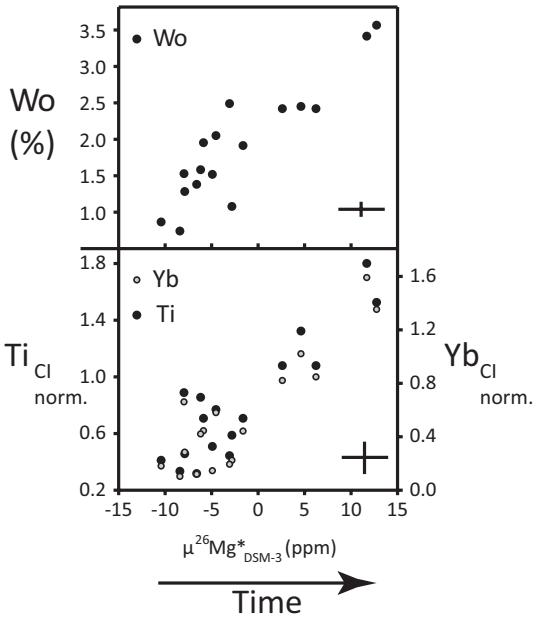

Fig. 5. Plot of Ti, Yb, and Wo content of orthopyroxenes in diogenites against bulk diogenite $\mu^{26}Mg^*$, reproduced from Schiller et al. (2011). $\mu^{26}Mg^*$ is a measure of excess ^{26}Mg produced by ^{26}Al decay in the first few million years of the solar system. Ti and Yb values are normalized to CI chondrites. Crosses represent analytical uncertainty (Schiller et al. 2011). Magma recharge can produce the large range in incompatible element concentrations, with values increasing over time as magma chambers become progressively enriched in incompatible elements.

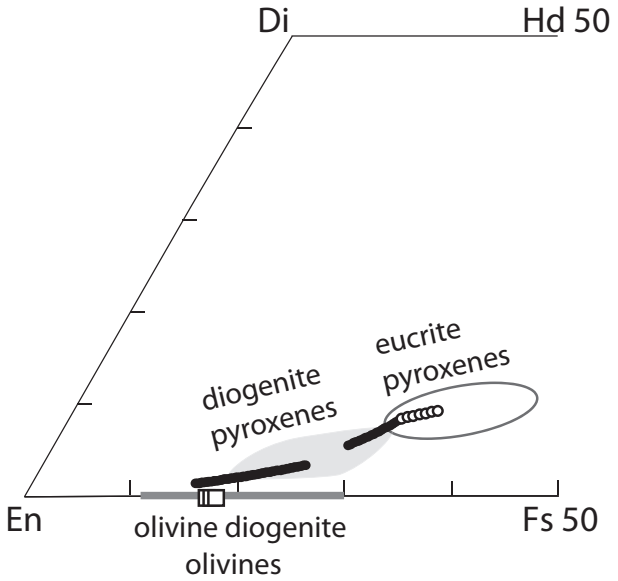

Fig. 6. Comparison of modeled mineral compositions (symbols) with observed compositions in HEDs (fields): olivine in dunite and olivine diogenites (open squares, dark gray field); pyroxene in diogenites (solid black circles, gray field); pyroxene in cumulate eucrites (open circles, open ellipse). Compositions are plotted in a portion of the pyroxene quadrilateral (En = $Mg_2Si_2O_6$, Fs 50 = $MgFeSi_2O_6$, Di = $CaMgSi_2O_6$, Hd 50 = $CaMg_{0.5}Fe_{0.5}Si_2O_6$). Fields are based largely on data from Mayne et al. (2009), Beck and McSween (2010) and Mittlefehldt et al. (2012). Additional data from clasts in howardite Y-7308 (Ikeda and Takeda 1985) provide a broader sampling of vestan lithologies.

and in some noncumulate eucrites (Barrat et al. 2007, 2010) could be that the magma chamber had experienced significant cumulate eucrite formation (producing a negative Eu anomaly), but was recharged such that it could crystallize diogenites and/or erupt eucritic liquids.

The Origin of Olivine-Bearing Diogenites

In this paper, we have chosen to reject an element of the proposed nomenclature of Beck and McSween (2010), in which they classify all diogenites with 10–90% olivine as harzburgitic diogenites or simply harzburgites. Although the general consensus is now that olivine-bearing diogenites are cumulates (see summary in McSween et al. 2013), many workers have discussed the possibility that olivine-rich diogenites represent partial melting residues in the vestan mantle because harzburgite is a common melting residue on Earth (e.g., Sack et al. 1991; McSween et al. 2013). This comparison can be confusing if the definition of harzburgite is not the same for both diogenites and terrestrial rocks; this is an issue that has previously been raised by Wittke et al. (2011).

The International Union of Geological Sciences (IUGS) classifies harzburgites as orthopyroxene + olivine rocks containing 40–90% olivine and <5% clinopyroxene (Streckeisen 1974; Fig. 7). This is a useful classification that was established because melting residues of any near-chondritic mantle will contain more than 40% olivine. If Vesta has a near-chondritic bulk composition in terms of major elements (Si, Al, Mg, Fe, Ca), it must have an olivine-rich deep mantle, which our models show to be a true harzburgite that forms by 60–70% crystallization of a magma ocean (Fig. 7). Diogenites with 10–40% olivine are not realistic candidates for this mantle because they have too little olivine. For the purposes of clarity and focus in the continued search for samples of Vesta's mantle, we choose to define harzburgites as recommended by the IUGS and Wittke et al. (2011). We use the term "olivine diogenite" to describe diogenites with <40% olivine, in line with the IUGS term "olivine pyroxenite" and in good agreement with the suggestions of Wittke et al. (2011).

For all of the successful models considered in this paper, the vestan mantle must contain >62% olivine (Fig. 7). Unless Vesta has a strongly nonchondritic

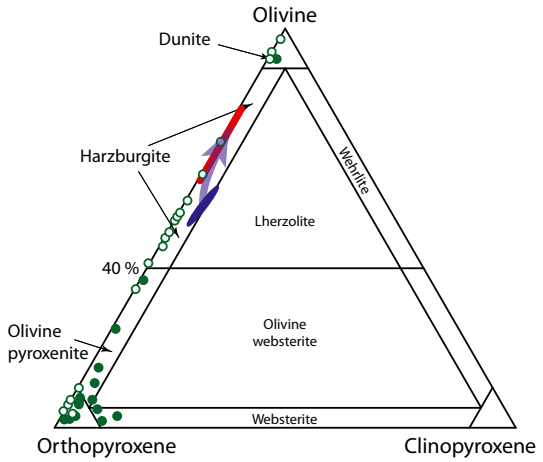

Fig. 7. Compositions of olivine-bearing diogenites with >1% olivine, plotted on the IUGS classification scheme for ultrabasic rocks with olivine + pyroxene >90% (Streckeisen 1974). Compositions represent averages if more than one sample of the same meteorite has been studied. Solid green circles represent literature data from Bowman et al. (1997), Righter (2001), Beck and McSween (2010), and Beck et al. (2011). Open green circles represent data from Wittke et al. (2011) and the Meteoritical Bulletin Database (http://www.lpi.usra.edu/meteor). Blue ellipse shows the range in normative mineralogy calculated for estimates of Vesta's bulk silicate composition (Table 1). This represents the approximate mineral assemblage that an undifferentiated vestan mantle would have. Arrow indicates the mineralogy of residues produced by either extracting a partial melt or extracting the residual melt after crystallization of a magma ocean, as in our models. Red region shows the range in mineralogy of the vestan mantle predicted by this study.

major-element composition, this is close to the minimum requirement for olivine content in the bulk of the vestan mantle. We therefore suggest that the search for samples of the vestan mantle should focus on samples with >60% olivine. However, most vestan dunites and harzburgitic diogenites probably represent olivine-rich cumulates formed in shallow magma chambers as a result of olivine-normative melt ascending from below, as seen in layered igneous intrusions on Earth (e.g., Irvine 1982). Samples with mineral compositions that plot on diogenite fractionation trends in terms of incompatible elements are especially likely to represent shallow cumulates, while samples with unusual compositions are more likely to represent the vestan mantle.

A More Complete Model

Figure 8 shows our model for heating, melting, cooling, and crystallization on Vesta, based on the results of our chemical models and existing physical models for magma oceans on Vesta and other planets/planetesimals. The early history of Vesta can be thought of in four stages:

Stage 1. Accretion and Heating: Development of a Magma Ocean

Vesta is assembled from smaller planetesimals. Many of these planetesimals are already hot or partly molten (Hevey and Sanders 2006). Vesta retains a primitive lid that is porous and insulating, but this porosity is rapidly reduced by sintering and self-compaction (Gupta and Sahijpal 2010). Heating by ^{26}Al causes extensive melting, allowing efficient sinking of iron into the growing core.

Stage 2. Surface Processing, Destruction of the Primitive Lid, and Rapid Cooling and Equilibrium Crystallization of the Magma Ocean

The thickness of the primitive lid is an important consideration because it exerts a first-order control on the rate at which Vesta heated and cooled. Early planetesimals were heated by ^{26}Al decay, but had a cold surface in contact with the interplanetary medium. Even when Vesta's interior had developed a convecting magma ocean, it should have retained a conductive lid.

Since the pioneering work of Ghosh and McSween (1998), thermal models of planetesimal heating have been largely based on solving the 1-D heat conduction equation (Merk et al. 2002; Hevey and Sanders 2006; Gupta and Sahijpal 2010; Elkins-Tanton et al. 2011; Moskovitz and Gaidos 2011; Neumann et al. 2012; Šrámek et al. 2012). All of these models attempt to incorporate some combination of other processes that affect the distribution of heat and rate of heat loss, such as continuous accretion (Merk et al. 2002; Gupta and Sahijpal 2010; Elkins-Tanton et al. 2011; Neumann et al. 2012; Šrámek et al. 2012), convection (Hevey and Sanders 2006; Gupta and Sahijpal 2010; Elkins-Tanton et al. 2011; Neumann et al. 2012), melt migration (Gupta and Sahijpal 2010; Moskovitz and Gaidos 2011; Neumann et al. 2012), sintering (Hevey and Sanders 2006; Gupta and Sahijpal 2010; Moskovitz and Gaidos 2011; Neumann et al. 2012), and even impacts (Šrámek et al. 2012). However, only the Gupta and Sahijpal (2010) and Elkins-Tanton et al. (2011) models deal with planetesimals that have radii larger than 120 km or smaller than 500 km (R_{Vesta} is approximately 270 km).

Understandably, no model adequately deals with heat loss from a convecting magma ocean on a Vesta-sized planetary embryo through a thin, dynamic lid that is subject to gravitational readjustment, penetration by impacts, advection of the melt to the surface, and periodic rapid radiative heat loss. However, the heat budget of growing planetesimals is strongly controlled by surface processes because all heat loss occurs at the surface. The thickness and processing of the cold lid are

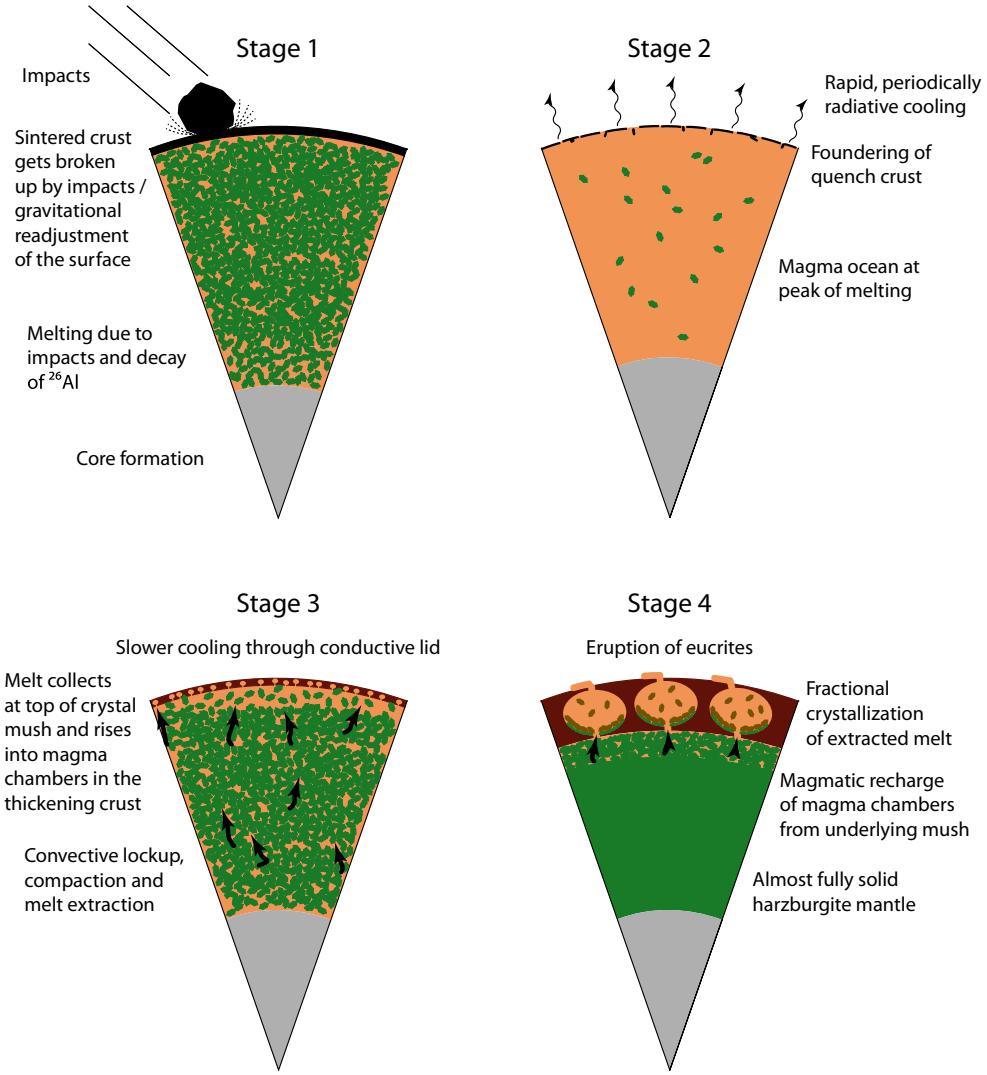

Fig. 8. Four-stage model for early melting and crystallization on Vesta. Crystals, magma chambers, and lava flows not to scale. See text for further details.

therefore vitally important for the thermal–chemical evolution of the asteroid.

A thin lid (<few km) would be easily broken up by impacts (e.g., Davison et al. 2012) and gravitational readjustment of the vestan surface. It would be prone to foundering and easily admixed into the magma ocean, which would expose hot magma ocean material to space. This would lead to rapid radiative cooling, as well as the formation of quench crust, which, being denser than the magma ocean, would itself founder into the interior (Walker et al. 1980), exposing more magma and forming more quench crust. This cycle, assisted by large impacts, would lead to rapid cooling of the magma ocean and very little preservation of compositional heterogeneity.

Conversely, a thicker lid (>10 km) would be porous and insulating, difficult to break up, and would inhibit the transport of magma to the surface due to its low density (Elkins-Tanton et al. 2011). The result would be slower cooling and the preservation of large-scale heterogeneity in the form of primitive chondritic material in the shallow vestan subsurface.

Understanding and quantifying the dynamics of the upper thermal boundary layer is an important next step for thermal models of asteroidal heating. However, for the immediate purposes of this study, we can take a broad look at lid behavior for Vesta. All caveats aside, the modeling results of Gupta and Sahijpal (2010) and Elkins-Tanton et al. (2011) indicate lid thicknesses that vary from approximately 1 to >25 km, depending on accretion time, accretion rate, and lid porosity. We can also take a simpler look at minimum lid thickness by using HED isotopic data to determine the timing of peak magma ocean conditions, and then deriving the lid thickness at this time from the conduction equation:

$$q = \frac{\kappa \Delta T}{z}$$

where q is heat flux at the surface, ΔT is the heat difference across the conductive lid (approximately 1500 K), κ is the thermal conductivity of the lid (approximately 1.5 W m^{-1} K^{-1}; Opeil et al. 2010), and z is the lid thickness. Peak magma ocean conditions on Vesta were likely reached approximately 2–3 Ma after CAIs (Lugmair and Shukolyukov 1998; Schiller et al. 2011). Adjusting heat production estimates for an asteroid composed of CI chondrites from Hevey and Sanders (2006) to account for the revised decay energy of Al^{26} (Castillo-Rogez et al. 2009) and the more Al-rich composition of Vesta compared with CI chondrites (Ghosh and McSween 1998), the total heat production on Vesta during peak magma ocean conditions was approximately 2.5–8 $\times$ 10^{12} W. Assuming a near-steady state magma ocean and lid temperature profile, this heat production rate corresponds to a surface heat flux of approximately 3–9 W m^{-2} during peak magma ocean conditions, which implies a lid thickness of 250–750 m. Although this is a crude estimate, this order of magnitude is reasonable if Vesta accreted early enough to reach peak magma ocean conditions by approximately 2 Ma after CAIs, for which there is ample chemical evidence (see the Chronology of Early Processes on Vesta section).

Gupta and Sahijpal (2010) and Schiller et al. (2011) note that a major difficulty in creating HEDs in a magma ocean scenario on Vesta is cooling the magma ocean rapidly enough. However, this is not an obstacle in the case of efficient lid removal and foundering of quench crust. The ancient HED ages are therefore not a problem for the time scales of thermal models.

The Vestan subsurface does not appear to contain a significant quantity of relict chondritic crust. Diogenites and most eucrites are homogeneous in their O isotopes (Greenwood et al. 2013), and very few contain any visible chondritic material (Zolensky et al. 1996). The presence of chondritic material in some howardites (Zolensky et al. 1996; Cartwright et al. 2012) and the observation of highly variable exotic material on the surface of Vesta (Reddy et al. 2012a) probably represent more recent impact delivery rather than a relict lid (Reddy et al. 2012a). The absence of relict lid material suggests a lid sufficiently thin (<few km) to be efficiently destroyed and reprocessed into the vestan interior during the magma ocean phase. This is broadly consistent with estimates from existing models and simple physical considerations.

Extensive processing of the surface and exposure of the magma ocean to space would result in rapid radiative cooling and equilibrium crystallization. Although a small amount of olivine settling was probably inevitable, the low gravity, relatively high convective velocities, and rapid solidification would severely limit settling. Furthermore, there is no robust evidence to suggest that the vestan magma ocean was ever above the liquidus, and only 70–80% melting is required to satisfy both isotopic homogeneity and core-mantle equilibria. If the vestan magma ocean retained at least a 10–20% crystal fraction at all stages, settling on a Myr time scale would have been essentially impossible due to crystal–crystal interactions (Suckale et al. 2012).

Stage 3. Convective Lockup and Melt Extraction

Our best-fit models require large-scale melt extraction from the magma ocean after 60–70% equilibrium crystallization. This is what the chemistry tells us, but the physical rationale for this process requires a brief consideration of crystal-liquid mixtures. The melt is more buoyant than the crystals (by approximately 450 kg m^{-3} in our models), so a crystal + liquid mush can only be maintained (i.e., melt extraction can only be prevented) if convection is sufficiently vigorous to mix the mush on a more rapid time scale than that of melt extraction.

Convection slows dramatically in a crystal suspension once crystals begin to interact with each other. For crystal shapes most relevant to an olivine + orthopyroxene crystal mush (crystal aspect ratio close to 1), an initial framework is generated at a crystal fraction of 20–30% (Saar et al. 2001; Baker et al. 2002; Walsh and Saar 2008). Above this crystal fraction, the mush has a yield strength, which increases near-exponentially as a function of crystal content until solid-like viscosities are reached at high crystal fractions (Walsh and Saar 2008). Modeling and experimental studies suggest that the rheology of the mush becomes overwhelmingly controlled by the rigid crystal framework at crystal fractions of 45–70% (Costa 2005; Costa et al. 2009, and references therein), dramatically increasing the viscosity and slowing convection.

Efficient melt extraction is possible once the buoyancy-driven ascent rate of melt exceeds the convective velocity of the system. This does not require convection to cease, but will instead occur below a critical convective velocity. Righter and Drake (1997) estimated that melt extraction would occur after 80% crystallization based on Kraichnan's (1962) condition for turbulent convection. Using the method of Righter and Drake (1997) for our model, we would obtain a critical crystal fraction of 74%. However, in Kraichnan's analysis, the turbulent regime does not suddenly switch from dominating the system to shutting off, but instead becomes infinitesimally small before disappearing. As such, the majority of the vestan

magma ocean would be in a viscous regime that permitted significant melt extraction before reaching this critical crystal fraction, even if a diminishing region in the center of the mush was still capable of turbulent convection. Removal of melt into shallow magma chambers would increase the crystal fraction in the mush, further promoting melt extraction and fully locking up the convective system.

After convective lockup, the quench-foundering cycle dramatically slows, thickening and stabilizing the lid, which results in slower cooling because the upper boundary of the system is now purely conductive. The convectively locked crystal framework slowly compacts as melt ascends out of it and into multiple adjacent (and possibly interacting) shallow magma chambers.

Stage 4. Fractional Crystallization in Shallow Magma Chambers and Eruption of Eucrites

Slow cooling allows fractional crystallization of the residual melt to produce diogenites and rare dunites, harzburgites, olivine diogenites, and cumulate eucrites. Magmatic recharge of magma chambers due to fluxing of more mafic melt from the underlying crystal mush maintains a narrow range of liquid compositions (Fig. 4b). These liquids are erupted to form noncumulate eucrites. Formation of cumulate eucrites is less efficient than formation of diogenites (Treiman 1997) due to the lower solid-melt density difference (approximately 200 kg m^{-3} for cumulate eucrites versus approximately 500 kg m^{-3} for diogenites: melt density approximately 2800 kg m^{-3}, plagioclase density approximately 2700 kg m^{-3}, pyroxene density approximately 3300 kg m^{-3}). As magmatic activity on Vesta wanes, any remaining melt in the magma chambers will crystallize as eucritic gabbros (Patzer and McSween 2012).

Predictions of Layer Thicknesses: Comparison with Dawn Data and Impact Modeling

Our model predicts crustal abundances of lithologies that distribute material in the vestan crust in a way that is consistent with the HED meteorite collection, most impact models, and Dawn observations. The general structure is an upper crust dominated by noncumulate eucrites and a lower crust dominated by accumulations of diogenite and rare interlayered cumulate eucrite, olivine diogenite, harzburgite, and dunite. Because magmatic transport is somewhat chaotic, the lithologies in the vestan crust will not be consistent in their lateral or vertical distribution. Some "lower crust" cumulate lithologies may be present in moderate quantities in the upper crust because individual magma chambers formed at different depths. However, we can provide some quantitative constraints on the general distribution of rock types. These are summarized in Fig. 9.

1. The vestan mantle is composed of harzburgite with 60–80% olivine.
2. The vestan crust is 30–41 km thick.
3. The vestan upper crust consists of 18–22 km of noncumulate eucrite.
4. The vestan lower crust consists of 13–19 km of cumulates. These are dominated by diogenite, but also include dunite, harzburgite, olivine diogenite, and cumulate eucrite. The total volume of cumulate eucrite represents a layer 1–2 km thick. The relative volumes of dunite, olivine diogenite, and diogenite are not independent and depend on the dynamics of magma recharge during crystallization. If all of the olivine is concentrated in a dunite layer, this layer should be 300–500 m thick. However, it is more likely that the olivine is more diffusely distributed in thin, cryptic layers of dunite, harzburgite, and olivine diogenite accounting for 10–20% of the lower crust. The total thickness of cumulate lithologies is more difficult to constrain than the noncumulate eucrite layer because it strongly depends on how crystalline the magma ocean was when melt extraction occurred.

The crust may be slightly thinner if melt extraction from the solidifying mantle was inefficient, or thicker if the bulk composition of Vesta is more silica-rich than the estimates we have used. From a simple mass balance, the crust cannot have an average thickness greater than 40–45 km if Vesta has a chondritic bulk composition. A thicker crust would be too mafic in composition to be the source of the HED meteorites.

The surface of Vesta consists largely of ejecta blankets and impact-processed regolith. The reprocessing of shallow vestan lithologies and admixing of impactor material (Cartwright et al. 2012) make it difficult to relate compositional variations on the surface of Vesta to lithological heterogeneity at depth. The best hope of understanding Vesta's shallow structure comes from the Rheasilvia impact basin. The impact that formed this basin is thought to have excavated the HED meteorites (Thomas et al. 1997), so these lithologies should be visible inside the basin. Dawn spectra indicate that Vesta's surface is composed of mixtures of eucritic and diogenitic material (De Sanctis et al. 2012). Inside the Rheasilvia impact basin, we would expect to see more exposure of the deep-seated lithologies, which is consistent with the observation of abundant diogenitic material in Rheasilvia (De Sanctis et al. 2012; Reddy et al. 2012b). Although the floor of the basin is likely a mess of debris from the impact itself (Jutzi and Asphaug 2011), the excavated lithologies should still be visible at the surface. Identification of diogenites in the Rheasilvia

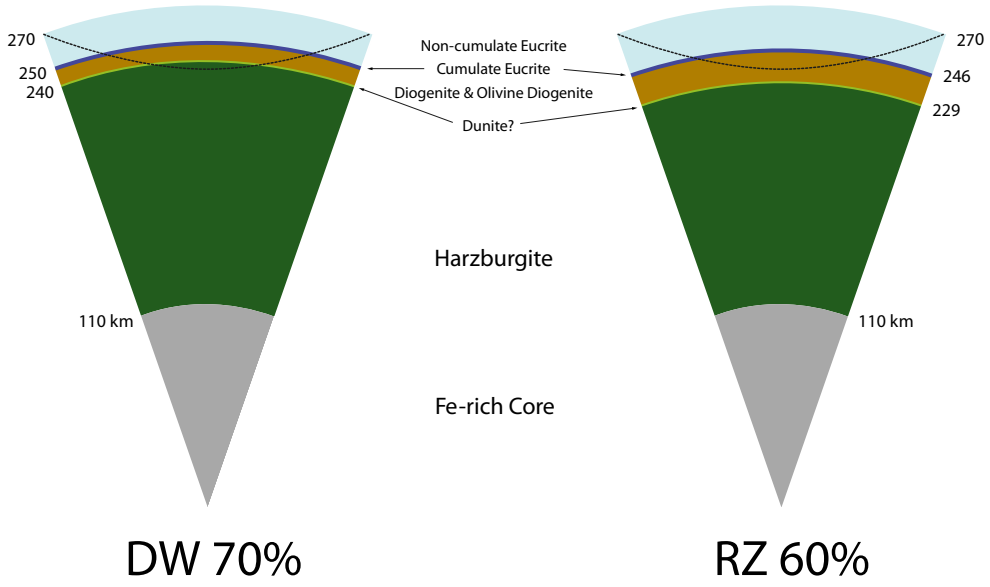

Fig. 9. Internal structure of Vesta as predicted by the two best-fit models from this study. Figures have been simplified to give a better indication of relative proportions of lithologies—in reality, the cumulate lithologies were probably formed in multiple overlapping magma chambers producing cryptically layered dunite, harzburgite, olivine diogenite, diogenite, and cumulate eucrite. Some of these magma chambers may have intruded the lower region of the noncumulate eucrite upper crust. The two models shown here represent near-end-member cases; to produce all HED lithologies, crustal thicknesses cannot be significantly less than 30 km or greater than 40 km. Dotted black line indicates an excavation depth of 35 km during formation of the Rheasilvia basin. See text for further details.

basin is further supported by measurements from Dawn's Gamma Ray and Neutron Detector (GRaND; Prettyman et al. 2012), although the low data resolution (many 10s of km) makes finer-scale analysis difficult.

McSween et al. (2013) report that spectral investigations of the Rheasilvia basin do not show any evidence for the presence of olivine. However, olivine diogenites with olivine contents <25% are spectrally indistinguishable from olivine-free diogenites (McSween et al. 2013), so the presence of olivine diogenite in the basin is entirely plausible. Furthermore, if olivine is present as dispersed, thin layers, then the resolution of Dawn's visible and infrared spectrometer (100s of meters) may not be able to resolve olivine-rich lithologies dispersed in the basin. However, the absence of large regions of olivine-rich lithologies in the Rheasilvia basin means that the impact cannot have significantly exposed the olivine-rich mantle. Hydrocode simulations of the Rheasilvia-forming impact have yielded estimated excavation depths of 30–50 km (Jutzi and Asphaug 2011; Ivanov and Melosh 2012). Our model predicts a crustal thickness of 30–41 km. This is consistent with the excavation of all of the HED lithologies (i.e., most of the crust) during the Rheasilvia-forming impact without exposing the olivine-rich mantle, provided the excavation depth is on the order of 40 km. Some excavation of olivine-rich mantle may be permitted if the exposed mantle is now covered by diogenitic and eucritic basin fill.

New simulations suggest that the combined maximum excavation depth of the two great south pole impact basins, Veneneia and Rheasilvia, is approximately 100 km (Jutzi et al. 2013). To explain the rarity of olivine on Vesta's surface, Jutzi and coworkers suggest that the outer 100 km of Vesta is composed of eucritic crust with diogenitic intrusions. It is important to emphasize here that this is not compatible with chondritic models of Vesta because a chondritic bulk Vesta cannot produce that much basaltic crust. There are three possible explanations for this: the simulations are incorrect, Vesta is not chondritic in composition (specifically, it must have a much higher Si/Mg ratio), or the impact excavated and ejected the olivine-rich mantle without depositing a lot of it back on the vestan surface.

CONCLUSIONS

1. We have explored a range of chemical models for the crystallization of a magma ocean on Vesta. The full range of igneous lithologies in the HED collection can be reproduced by a two-step model that invokes 60–70% equilibrium crystallization of a magma ocean at 500 bars average pressure (approximately 60 km depth), followed by extraction of this melt from a convectively locked crystal network and subsequent fractional crystallization of this melt in shallower magma chambers.

2. The narrow range in eucrite compositions can be produced by recharge of shallow magma chambers by melt ascending from the underlying crystal mush. Magmatic recharge can also explain the wide range of incompatible minor and trace element concentrations in diogenites and their correlation with age.
3. Vesta's mantle is composed of harzburgite with 60–80% olivine. Vesta's crust is 30–41 km thick. The upper 18–22 km consists of noncumulate eucrite. The lower crust is dominated by diogenite, but includes 10–20% each of olivine-bearing diogenite and cumulate eucrite. The distribution of lithologies is crudely layered, but laterally and vertically heterogeneous.
4. Our model predicts a crustal structure that is consistent with both Dawn observations and most impact models of the Rheasilvia basin. All of the HED lithologies could have been excavated during the impact that formed the Rheasilvia basin without exposing olivine-rich mantle as long as the excavation depth did not significantly exceed 40 km. The recent suggestion of Jutzi et al. (2013) that Vesta's crust is 100 km thick would require the bulk composition of Vesta to be strongly nonchondritic.

Acknowledgments—This work was funded by NSF Astronomy grant 0747154 to L. T. Elkins-Tanton and NASA grant NNX12AH80G to T. L. Grove. A number of the ideas in this paper were crystallized and refined through discussions with T. Grove, J.-A. Olive, and R. Fu. This manuscript was substantially improved thanks to reviews by K. Righter, G. J. Taylor, and an anonymous reviewer.

DISCLOSURE STATEMENT

The authors declare no conflicts of interest.

Editorial Handling—Dr. Hap McSween

REFERENCES

Aitchison J. 1986. *The statistical analysis of compositional data*. London: Chapman Hall Ltd. 416 p.

Asimow P. D. and Ghiorso M. S. 1998. Algorithmic modifications extending MELTS to calculate subsolidus phase relations. *American Mineralogist* 83:1127–1131.

Baker D. R., Paul G., Sreenivasan S., and Stanley H. E. 2002. Continuum percolation threshold for interpenetrating squares and cubes. *Physical Review E* 66:046136.

Barrat J.-A., Yamaguchi A., Greenwood R. C., Bohn M., Cotton J., Benoit M., and Franchi I. A. 2007. The Stannern trend eucrites: Contamination of main group eucritic magmas by crustal partial melts. *Geochimica et Cosmochimica Acta* 71:4108–4124.

Barrat J.-A., Yamaguchi A., Greenwood R. C., Benoit M., Cotten J., Bohn M., and Franchi I. A. 2008. Geochemistry of diogenites: Still more diversity in their parental melts. *Meteoritics & Planetary Science* 43:1759–1775.

Barrat J.-A., Yamaguchi A., Zanda B., Bollinger C., and Bohn M. 2010. Relative chronology of crust formation on asteroid Vesta: Insights from the geochemistry of diogenites. *Geochimica et Cosmochimica Acta* 74:6218–6231.

Beck A. W. and McSween H. Y. 2010. Diogenites as polymict breccias composed of orthopyroxenite and harzburgite. *Meteoritics & Planetary Science* 45:850–872.

Beck A. W., Mittlefehldt D. W., McSween H. Y., Rumble D., Lee C.-T. A., and Bodnar R. J. 2011. MIL 03443, a dunite from asteroid 4 Vesta: Evidence for its classification and cumulate origin. *Meteoritics & Planetary Science* 46:1133–1151.

Binzel R. P. and Xu S. 1993. Chips of asteroid 4 Vesta: Evidence for the parent body of basaltic achondrite meteorites. *Science* 260:186–191.

Blichert-Toft J., Boyet M., Philippe T., and Albarède F. 2002. ^{147}Sm-^{143}Nd and ^{176}Lu-^{176}Hf in eucrites and the differentiation of the HED parent body. *Earth and Planetary Science Letters* 204:167–181.

Boesenberg J. S. and Delaney J. S. 1997. A model composition of the basaltic achondrite planetoid. *Geochimica et Cosmochimica Acta* 61:3205–3225.

Bogard D. D. and Garrison D. H. 2003. ^{39}Ar-^{40}Ar ages of eucrites and thermal history of asteroid 4 Vesta. *Meteoritics & Planetary Science* 38:669–710.

Bowman L. E., Spilde M. N., and Papike J. J. 1997. Automated energy-dispersive spectrometer modal analysis applied to the diogenites. *Meteoritics & Planetary Science* 32:869–875.

Cartwright J. A., Mittlefehldt D. W., Quinn J. E., and Ott U. 2012. The continuing quest for "regolithic" howardites (abstract #1211). 43rd Lunar and Planetary Science Conference. CD-ROM.

Castillo-Rogez J., Johnson T. V., Lee M. H., Turner N. J., Matson D. L., and Lunine J. 2009. ^{26}Al decay: Heat production and a revised age for Iapetus. *Icarus* 204:658–662.

Clayton R. N. and Mayeda T. K. 1988. Formation of ureilites by nebular processes. *Geochimica et Cosmochimica Acta* 52:1313–1318.

Costa A. 2005. Viscosity of high crystal content melts: Dependence on solid fraction. *Geophysical Research Letters* 32:L22308.

Costa A., Caricchi L., and Bagdassarov N. 2009. A model for the rheology of particle-bearing suspensions and partially molten rocks. *Geochemistry Geophysics Geosystems* 10: Q03010.

Davison T. M., Ciesla F. J., and Collins G. S. 2012. Post-impact thermal evolution of porous planetesimals. *Geochimica et Cosmochimica Acta* 95:252–269.

DePaolo D. J. 1981. Trace element and isotopic effects of combined wallrock assimilation and fractional crystallization. *Earth and Planetary Science Letters* 53:189–202.

De Sanctis M. C., Ammannito E., Capria M. T., Tosi F., Capaccioni F., Zambon F., Carraro F., Fonte S., Frigeri A., Jaumann R., Magni G., Marchi S., McCord T. B., McFadden L. A., McSween H. Y., Mittlefehldt D. W., Nathues A., Palomba E., Pieters C. M., Raymond C. A., Russell C. T., Toplis M. J., and Turrini D. 2012. Spectroscopic characterization of mineralogy and its diversity across Vesta. *Science* 336:697–700.

Dreibus G. and Wänke H. 1980. The bulk composition of the eucrite parent asteroid and its bearing on planetary evolution. *Zeitschrift für Naturforschung* 35a:204–216.

Elkins-Tanton L. T., Weiss B. P., and Zuber M. T. 2011. Chondrites as samples of differentiated planetesimals. *Earth and Planetary Science Letters* 305:1–10.

Fowler G. W., Papike J. J., Spilde M. N., and Shearer C. K. 1995. Diogenites as asteroidal cumulates: Insights from orthopyroxene major and minor element chemistry. *Geochimica et Cosmochimica Acta* 58:3921–3929.

Ghiorso M. S. and Sack R. O. 1995. Chemical mass transfer in magmatic processes IV. A revised and internally consistent thermodynamic model for the interpolation and extrapolation of liquid-solid equilibria in magmatic systems at elevated temperatures and pressures. *Contributions to Mineralogy and Petrology* 119:197–212.

Ghosh A. and McSween H. Y. 1998. A thermal model for the differentiation of asteroid 4 Vesta, based on radiogenic heating. *Icarus* 134:187–206.

Greenwood R. C., Barrat J.-A., Scott E. R. D., Franchi I. A., Yamaguchi A., Gibson J. M., Haack H., Lorenz C. A., Ivanova M. A., and Bevan A. 2013. Large-scale melting and impact mixing on early-formed asteroids: Evidence from high-precision oxygen isotope studies (abstract #3048). 44th Lunar and Planetary Science Conference. CD-ROM.

Grove T. L. and Bartels K. S. 1992. The relation between diogenite cumulates and eucrite magmas. Proceedings, 22nd Lunar and Planetary Science Conference. pp. 437–445.

Gupta G. and Sahijpal S. 2010. Differentiation of Vesta and the parent bodies of other achondrites. *Journal of Geophysical Research* 115:E08001.

Hevey P. J. and Sanders I. S. 2006. A model for planetesimal meltdown by ^{26}Al and its implications for meteorite parent bodies. *Meteoritics & Planetary Science* 41:95–106.

Ikeda Y. and Takeda H. 1985. A model for the origin of basaltic achondrites based on the Yamato 7308 howardite. *Journal of Geophysical Research* 90:C649–C663.

Irvine T. N. 1982. Terminology for layered intrusions. *Journal of Petrology* 23:127–162.

Ivanov B. A. and Melosh H. J. 2012. The Rheasilvia crater on Vesta: Numerical modeling (abstract #2148). 43rd Lunar and Planetary Science Conference. CD-ROM.

Jutzi M. and Asphaug E. 2011. Mega-ejecta on asteroid Vesta. *Geophysical Research Letters* 38:L01102.

Jutzi M., Asphaug E., Gillet P., Barrat J.-A., and Benz W. 2013. The structure of the asteroid 4 Vesta as revealed by models of planet-scale collisions. *Nature* 494:207–210.

Kitts K. and Lodders K. 1998. Survey and evaluation of eucrite bulk compositions. *Meteoritics & Planetary Science* 33:A197–A213.

Kleine T., Mezger K., Palme H., Scherer E., and Münker C. 2005. The W isotope composition of eucrite metals: Constraints on the timing and cause of the thermal metamorphism of basaltic eucrites. *Earth and Planetary Science Letters* 231:41–52.

Kraichnan R. H. 1962. Turbulent thermal convection at arbitrary Prandtl number. *Physics of Fluids* 5:1374–1389.

Lodders K. 2000. An oxygen isotope mixing model for the accretion and composition of rocky planets. *Space Science Reviews* 92:341–354.

Lugmair G. W. and Shukolyukov A. 1998. Early solar system timescales according to ^{53}Mn-^{53}Cr systematics. *Geochimica et Cosmochimica Acta* 62:2863–2886.

Mayne R. G., McSween H. Y., McCoy T. H., and Gale A. 2009. Petrology of the unbrecciated eucrites. *Geochimica et Cosmochimica Acta* 73:794–819.

McCord T. B., Adams J. B., and Johnson T. V. 1970. Asteroid Vesta: Spectral reflectivity and compositional implications. *Science* 168:1445–1447.

McSween H. Y., Mittlefehldt D. W., Beck A. W., Mayne R. G., and McCoy T. J. 2011. HED meteorites and their relationship to the geology of Vesta and the Dawn mission. *Space Science Reviews* 163:141–174.

McSween H. Y., Ammannito E., Reddy V., Prettyman T. H., Beck A. W., De Sanctis M. C., Nathues A., Le Corre L., O'Brien D. P., Yamashita N., McCoy T. J., Mittlefehldt D. W., Toplis M. J., Schenk P., Palomba E., Turrini D., Tosi F., Zambon F., Longobardo A., Capaccioni F., Raymond C. A., and Russell C. T. 2013. Composition of the Rheasilvia basin, a window into Vesta's interior. *Journal of Geophysical Research* 118:335–346, doi:10.1002/jgre.20057

Merk R., Breuer D., and Spohn T. 2002. Numerical modeling of ^{26}Al-induced radioactive melting of asteroids considering accretion. *Icarus* 159:183–191.

Misawa K., Yamaguchi A., and Kaiden H. 2005. U-Pb and ^{207}Pb-^{206}Pb ages of zircons from basaltic eucrites: Implications for early basaltic volcanism on the eucrite parent body. *Geochimica et Cosmochimica Acta* 69:5847–5861.

Mittlefehldt D. W. 1994. The genesis of diogenites and HED parent body petrogenesis. *Geochimica et Cosmochimica Acta* 58:1537–1552.

Mittlefehldt D. W., Beck A. W., Lee C.-T. A., McSween H. Y., and Buchanan P. C. 2012. Compositional constraints on the genesis of diogenites. *Meteoritics & Planetary Science* 47:72–98.

Moskovitz N. and Gaidos E. 2011. Differentiation of planetesimals and the thermal consequences of melt migration. *Meteoritics & Planetary Science* 46:903–918.

Neumann W., Breuer D., and Spohn T. 2012. Differentiation and core formation in accreting planetesimals. *Astronomy & Astrophysics* 543:A141.

Nyquist L. E., Takeda H., Shih C.-Y., and Wiesmann H. 2004. Sm-Nd age and initial ^{87}Sr/^{86}Sr for Yamato 980318: an old cumulate eucrite (abstract #1330). 35th Lunar and Planetary Science Conference. CD-ROM.

O'Hara M. J. 1977. Geochemical evolution during fractional crystallization of a periodically refilled magma chamber. *Nature* 266:503–507.

Opeil C. P., Consolmagno G. J., and Britt D. T. 2010. The thermal conductivity of meteorites: New measurements and analysis. *Icarus* 208:449–454.

Palme H. and Rammensee W. 1981. The significance of W in planetary differentiation processes: Evidence from new data on eucrites. Proceedings, 12th Lunar and Planetary Science Conference. pp. 949–964.

Palme H., Baddenhausen H., Blum K., Cendales M., Dreibus G., Hofmeister H., Kruse H., Palme C., Spettel B., Vilcsek E., Wanke H., and Kurat G. 1978. New data on lunar samples and achondrites and a comparison of the least fractionated samples from the Earth, the Moon and the eucrite parent body. Proceedings, 9th Lunar and Planetary Science Conference. pp. 25–57.

Patzer A. 2013. New data on the chemical compositions of silicates in HED meteorites: Variety is the spice (abstract #2468). 44th Lunar and Planetary Science Conference. CD-ROM.

Patzer A. and McSween H. Y. 2012. Gabbroic vs. cumulate eucrites: Extending the diversity of eucritic lithologies (abstract #1227). 43rd Lunar and Planetary Science Conference. CD-ROM.

Prettyman T. H., Mittlefehldt D. W., Yamashita N., Lawrence D. J., Beck A. W., Feldman W. C., McCoy T. J., McSween H. Y., Toplis M. J., Titus T. N., Tricarico P., Reedy R. C., Hendricks J. S., Forni O., Le Corre L., Li J.-Y., Mizzon H., Reddy V., Raymond C. A., and Russell C. T. 2012. Elemental mapping by Dawn reveals exogenic H in Vesta's regolith. *Science* 338:242–246.

Quitté G., Latkoczy C., Schönbächler M., Halliday A. N., and Günther D. 2011. ^{60}Fe-^{60}Ni systematics in eucrite parent body: A case study of Bouvante and Juvinas. *Geochimica et Cosmochimica Acta* 75:7698–7706.

Reddy V., Le Corre L., O'Brien D. P., Nathues A., Cloutis E. A., Durda D. D., Bottke W. F., Bhatt M. U., Nesvorny D., Buczkowski D., Scully J. E. C., Palmer E. M., Sierks H., Mann P. J., Becker K. J., Beck A. W., Mittlefehldt D. W., Li J.-Y., Gaskell R., Russell C. T., Gaffey M. J., McSween H. Y., McCord T. B., Combe J. P., and Blewett D. Delivery of dark material to Vesta via carbonaceous chondrite impacts. *Icarus* 221:544–559.

Reddy V., Nathues A., Le Corre L., Sierks H., Li J.-Y., Gaskell R., McCoy T., Beck A. W., Schroder S. E., Pieters C. M., Becker K. J., Buratti B. J., Denevi B., Blewett D. T., Christensen U., Gaffey M. J., Gutierrez-Marques P., Hicks M., Keller H. U., Maue T., Mottola S., McFadden L. A., McSween H. Y., Mittlefehldt D., O'Brien D. P., Raymond C., and Russell C. 2012b. Color and albedo heterogeneity of Vesta from Dawn. *Science* 336:700–704.

Righter K. 2001. Petrography, mineralogy and petrology of two new HED meteorites: Diogenite GRA 98108 and howardite GRA 98030 (abstract #1765). 32nd Lunar and Planetary Science Conference. CD-ROM.

Righter K. and Drake M. J. 1997. A magma ocean on Vesta: Core formation and petrogenesis of eucrites and diogenites. *Meteoritics & Planetary Science* 32:929–944.

Ruzicka A., Snyder G. A., and Taylor L. A. 1997. Vesta as the howardite, eucrite and diogenite parent body: Implications for the size of a core and for large scale differentiation. *Meteoritics & Planetary Science* 32:825–840.

Saar M. O., Manga M., Cashman K. V., and Fremouw S. 2001. Numerical models of the onset of yield strength in crystal-melt suspensions. *Earth and Planetary Science Letters* 187:367–379.

Sack R. O., Azeredo W. J., and Lipschutz M. E. 1991. Olivine diogenites: The mantle of the eucrite parent body. *Geochimica et Cosmochimica Acta* 55:1111–1120.

Schiller M., Baker J., Creech J., Paton C., Millet M.-A., Irving A., and Bizzarro M. 2011. Rapid timescales for magma ocean crystallization on the howardite-eucrite-diogenite parent body. *The Astrophysical Journal Letters* 740:L22.

Shearer C. K., Fowler G. W., and Papike J. J. 1997. Petrogenetic models for magmatism on the eucrite parent body: Evidence from orthopyroxene in diogenites. *Meteoritics & Planetary Science* 32:877–889.

Shearer C. K., Burger P., and Papike J. J. 2010. Petrogenetic relationships between diogenites and olivine diogenites: Implications for magmatism on the HED parent body. *Geochimica et Cosmochimica Acta* 74:4865–4880.

Shukolyukov A. and Lugmair G. W. 1993. ^{60}Fe in eucrites. *Earth and Planetary Science Letters* 119:159–166.

Singletary S. J. and Grove T. L. 2003. Early petrologic processes on the ureilite parent body. *Meteoritics & Planetary Science* 38:95–108.

Šrámek O., Milelli L., Ricard Y., and Labrosse S. 2012. Thermal evolution and differentiation of planetesimals and planetary embryos. *Icarus* 217:339–354.

Stolper E. 1975. Petrogenesis of eucrite, howardite and diogenite meteorites. *Nature* 258:220–222.

Stolper E. 1977. Experimental petrology of eucritic meteorites. *Geochimica et Cosmochimica Acta* 41:587–611.

Streckeisen A. 1974. Classification and nomenclature of plutonic rocks. *Geologische Rundschau* 63:773–785.

Suckale J., Sethian J. A., Yu J.-D., and Elkins-Tanton L. T. 2012. Crystals stirred up: 1. Direct numerical simulations of crystal settling in nondilute magmatic suspensions. *Journal of Geophysical Research* 117: E08004.

Tait S. R. and Jaupart C. 1996. The production of chemically stratified and adcumulate plutonic igneous rocks. *Mineralogical Magazine* 60:99–114.

Tait S. R., Huppert H. E., and Sparks R. S. J. 1984. The role of compositional convection in the formation of adcumulate rocks. *Lithos* 17:139–146.

Thomas P. E., Binzel R. P., Gaffey M. J., Storrs A. D., Wells E. N., and Zellner B. H. 1997. Impact excavation on asteroid 4 Vesta: Hubble Space Telescope results. *Science* 277:1492–1495.

Treiman A. H. 1997. The parent magmas of the cumulate eucrites: A mass balance approach. *Meteoritics & Planetary Science* 32:217–230.

Trinquier A., Birck J.-L., Allègre C. J., Göpel C., and Ulfbeck D. 2008. ^{53}Mn-^{53}Cr systematics of the early solar system revisited. *Geochimica et Cosmochimica Acta* 72: 5146–5163.

Walker D., Hager B. H., and Hays J. F. 1980. Mass and heat transport in a lunar magma ocean by sinking blobs. Proceedings, 11th Lunar and Planetary Science Conference. pp. 1196–1198.

Walsh S. D. C. and Saar M. O. 2008. Numerical models of stiffness and yield stress growth in crystal-melt suspensions. *Earth and Planetary Science Letters* 267:32–44.

Wänke H., Baddenhausen H., Balacescu A., Teschke F., Spettel B., Dreibus G., Palme H., Quijano-Rico M., Kruse H., Wlotzka F., and Begemann F. 1972. Multielement analyses of lunar samples and some implications of the results. Proceedings, 3rd Lunar and Planetary Science Conference. pp. 1251–1268.

Warren P. H. 1997. Magnesium oxide-iron oxide mass balance constraints and a more detailed model for the relationship between eucrites and diogenites. *Meteoritics & Planetary Science* 32:945–963.

Wittke J. H., Irving A. J., Bunch T. E., and Kuehner S. M. 2011. A nomenclature system for diogenites consistent with the IUGS system for naming terrestrial ultramafic rocks (abstract #5223). 74th Annual Meteoritical Society Meeting, London, UK.

Zhang J., Dauphas N., Davis A. M., Leya I., and Fedkin A. 2012. The proto-Earth as a significant source of lunar material. *Nature Geoscience* 5:251–255.

Zolensky M. E., Weisberg M. K., Buchanan P. C., and Mittlefehldt D. W. 1996. Mineralogy of carbonaceous chondrite clasts in HED achondrites and the Moon. *Meteoritics & Planetary Science* 31:518–537.